Extended Abstract

New Sulfides for Thermoelectric Applications

Helena da Conceição Maçarico Ferreira
helena.ferreira@tecnico.ulisboa.pt
Instituto Superior Técnico, Lisbon, Portugal
June 2019

Abstract

Current commercially available thermoelectric materials contain rare, expensive and toxic elements, demanding for new, cheap, abundant and environment-friendly alternatives, such as some metal sulfides. This work consists in the preparation of FeS_2 (pyrite), NiS_2 (vaesite) and CoSbS (paracostibite), by solid state techniques at high temperatures followed by hot-pressing, and heat treatment. Pyrite and paracostibite with modified chemical compositions were also prepared. The crystal structure, chemical composition, thermal stability, electronic band structure and transport properties were characterized. Single phase pyrite and vaesite were obtained. Paracostibite had smaller amounts of β-CoS, even after heat-treatment. High relative densities were achieved (>90%). No significant lattice distortions were detected for different hot-pressing conditions. However, modifications of the initial composition promoted lattice disorder. Thermogravimetric analysis showed a strong desulfurization above 340ºC for pyrite and vaesite, and 800ºC for paracostibite. The negative Seebeck coefficient in pyrite, suggesting n-type semiconductivity, contradicts first-principle calculations (p-type). A maximum power factor (300K) of 0.2 $\mu WK^{-2}m^{-1}$ was obtained for pristine pyrite, and 105.5 $\mu WK^{-2}m^{-1}$ for pyrite with Co and Se. DFT calculations of vaesite electronic structure suggest metallic behaviour, whereas experimental results showed n-type semiconductivity. A maximum power factor (300K) was 14.1 $\mu WK^{-2}m^{-1}$ was obtained. Paracostibite reached a maximum power factor (300K) of 72 $\mu WK^{-2}m^{-1}$, when Ni is added to the composition. Its negative Seebeck coefficient also contradicts DFT calculations, that suggest p-type semiconductivity. These results are a good starting point for further improvement of the thermoelectric properties, with a proper optimization of the chemical composition and microstructure.

Keywords: Thermoelectric materials, sulfides, pyrite, vaesite, paracostibite, power factor

---

1. Introduction

The search for new clean energy sources, as well as the optimization of the existing ones, has become a major issue in contemporary societies. According to the World Energy Council, current conventional thermal power plants have an energy efficiency around 35-45%, most of the energy being lost as wasted heat [1]. Thermoelectric (TE) materials are a promising solution to increase the efficiency in many devices, due to their capability to convert thermal energy into electric energy (Seebeck effect), and vice-versa (Peltier effect). The potential of a material to be used in thermoelectric applications is evaluated by its figure of merit, $zT = \alpha^2 T/\rho\lambda$, where α, T, ρ and λ are the Seebeck coefficient, absolute temperature, electrical

resistivity and thermal conductivity, respectively [2].

Current commercially available TE materials, such as Bi_2Te_3 and PbTe, contain rare, expensive and toxic elements. Thus, it is necessary to develop new, cheap, abundant and environment-friendly alternatives. Metal sulfides are interesting candidates, as they fulfill these requirements [3]. In this work, it was explored the potential of three minerals - FeS_2, NiS_2 and CoSbS – as thermoelectric materials. Pyrite and vaesite are transition metal chalcogenides with cubic structure (Pa3) and semiconducting behavior [4, 5]. Previous studies regarding pyrite TE properties reveal a modest power factor, high thermal conductivity and low zT at room temperature [6] . To the best of our knowledge, no measurements of electrical properties on bulk NiS_2 or thermal conductivity have been reported. Thermoelectric measurements showed a low power factor at room temperature for thin films (0.12 $\mu WK^{-2}m^{-1}$), being substantially higher in single crystals (5-16 $\mu WK^{-2}m^{-1}$) [7, 8]. Paracostibite has an orthorhombic structure (Pbca) [9] and its thermoelectric properties have been under focus, due to the high power factors of bulk samples at room temperature (up to 75 $\mu WK^{-2}m^{-1}$), synthesized by spark plasma sintering [10, 11, 12, 13]. All these sulfides seem promising, since several strategies that could lead to a significant improvement of their TE performance remain unexplored.

This work consists in the preparation of FeS_2, NiS_2 and CoSbS, by solid state techniques at high temperatures (800ºC) followed by hot-pressing, and heat treatment when necessary. Several modifications of pyrite and paracostibite initial chemical compositions were also prepared, with partial substitution of the metallic cation and substitution of sulfur by selenium. Afterwards, the samples were characterized in terms of chemical composition and microstructure (XRD, optical and electron microscopy, EDS, Raman spectroscopy, density measurements), thermal stability (TGA), and electronic transport properties (DFT electronic structure calculations, Seebeck coefficient and electrical resistivity).

2. Experimental Procedure and Techniques

Samples with ~1.5g were prepared by reacting the starting elements in evacuated quartz ampoules. An excess of 5wt% of the chalcogenide elements was added to compensate evaporation during ampoule sealing. The ampoules were submitted to an initial heating cycle at 800 ºC for 12 h, with a heating speed of 0.3ºC/min and two intermediate dwells at 400 ºC and 650 ºC for 8 h. Pyrite with Co or Ni were heated, in the same conditions, but only up to 650ºC.

The samples were slowly cooled inside the furnace, manually ground, cold pressed, sealed in evacuated quartz ampoules and heated again in the same conditions. The samples were manually powdered, an excess of 30wt% (pyrite and vaesite) or 15wt% (paracostibite) of chalcogenide elements was added. The powders were hot-pressed in graphite molds, at several consolidation conditions. CoSbS required a final heat treatment (at 720ºC for 7 days in an evacuated quartz ampoule, quenched in water) to eliminate secondary phases. The processing history of each sample is described in Table 1.

Part of each pellet was manually ground and characterized by powder X-ray diffraction (XRD). A PANalytical X'Pert PRO diffractometer (Bragg-Brentano geometry, Cu Kα radiation) was used.

The powders were placed in a low-noise Si single crystal XRD holder and 2θ was scanned from 10º to 90º, with a step size of 0.033º and a time per step of 50.165 s. Cell parameters and theoretical density were calculated and refined from the powder diffraction data, using UnitCell software [14]. Apparent density was determined by the Archimedes method. Porosity and volume percentage were estimated by image analysis (ImageJ).

Table 1 – Summary of sample preparation and processing. *All samples were hot-pressed for 1.5h, except for CoSbS-based compounds (1.25h).

Sample	Nominal composition	Preparation	Hot-pressing*		Heat-treatm.
p-FeS_2_1	FeS_2	2x heat-treated at 800ºC, 12h	FeS_2_525_49	525ºC, 49MPa, 1.5h	No
			FeS_2_710_39	710ºC, 39MPa, 1.5h	
p-FeS_2_2		2x heat-treated at 650ºC, 12h	FeS_2_710_49	710ºC, 49MPa, 1.5h	
			FeS_2_710_60	710ºC, 60MPa, 1.5h	
(Co,Se)-FeS_2	$Fe_{0.9}Co_{0.1}S_{1.75}Se_{0.25}$		710ºC, 49MPa, 1.5h		
(Ni,Se)-FeS_2	$Fe_{0.9}Ni_{0.1}S_{1.75}Se_{0.25}$		710ºC, 49MPa, 1.5h		
p-NiS_2	NiS_2	2x heat-treated at 800ºC, 12h	NiS_2_700_56	700ºC, 56MPa, 1.5h	
			NiS_2_720_56	720ºC, 56MPa, 1.5h	
			NiS_2_750_56	720ºC, 56MPa, 1.5h	
p-CoSbS	CoSbS		725ºC, 49MPa, 1.25h		720ºC, 7 days
Ni-CoSbS	$Co_{0.95}Ni_{0.05}SbS$				
Se-CoSbS	$CoSbS_{0.9}Se_{0.1}$				

Optical microscopy, scanning electron microscopy (SEM) and energy-dispersive spectroscopy (EDS) were used for microstructure characterization and chemical composition analysis. It was used an optical microscope ZEISS SteREO Discovery V20 and a JEOL JSM-7001F field emission gun scanning electron microscope (accelerating voltage of 25kV), with an Oxford Instruments EDS spectroscopy system attached.

Thermal stability was evaluated with thermogravimetric analysis (TGA). A Dupont 951 and a TG Q500 thermo-gravimetric analyzers were used for FeS_2 and NiS_2 and a Setaram Labsys TG-DTA/DSC was used for CoSbS. Samples were manually grounded, placed in platinum or alumina pans, and heated from 25ºC to 950ºC, at a heating rate of 10ºC/min in an inert atmosphere flowing at a rate of 60mL/min.

The chemical bonding was analyzed by Raman spectroscopy, using a Horiba LabRam HR Evolution Raman microspectometer (laser with λ=532 nm and 10mW power). Raman spectra were collected from 150 to 1800 cm^{-1}, with the laser light focused with a 100x objective. 4 scans, with 30 seconds each, were made for each spectrum. Lower laser powers (25-50% of maximum) were required in some samples to avoid the surface damage.

Electrical transport properties were measured between 20-300K, at a rate of 0.3K/min for the Seebeck coefficient and 0.5K/min for electrical resistivity, using a closed-cycle cryostat. A system based on the Chaikin's device to measure organic single crystals was used to

measure the Seebeck coefficient [15]. The samples were first shaped to a needle-like geometry (~0.5x0.5x3.5mm) and placed between two gold foils (located in two single crystal quartz blocks attached to a temperature-controlled heat sink in order to be heated independently), with the tips glued to the foils with cryogenic varnish. Two gold wires connected the sample and the quartz blocks, to establish electrical and thermal contacts. The voltage was measured with a low frequency AC technique, with a maximum temperature gradient in the sample of 1K, controlled by two Au-Fe-Chromel thermocouples connected to the quartz blocks. The electrical resistivity was measured in the same needle-like shape (~1x1x3mm) through the four-point technique, using an AC resistance bridge and a current of 1mA.

The band structure and density of states of FeS_2, NiS_2 and CoSbS were calculated with WIEN2k package [16]. Calculations were performed within the density functional theory (DFT), using linear augmented plane wave (LAPW) method to solve the Kohn-Sham equations. Lattice parameters and atomic positions were taken from experimental data [17]. It was adopted both LSDA and GGA+mBJ methods, with PBE parametrization, to approximate the exchange-correlation functional [18]. A cut-off energy of 6 Ry and 1000 k-points in the irreducible part of the Brillouin zone were used for the self-consistent calculations. The criterium of convergence was set at 0.0001 Ry. A simple cubic Brillouin zone was used for FeS_2 and NiS_2, and an orthorhombic for CoSbS.

3. Results and discussion

3.1. Preparation by solid state reaction

Two solid-state reactions were required to obtain (mostly) single phase compounds. The XRD diffractogram of NiS_2 exhibits no secondary phases after the second heating cycle. In pyrite XRD diffractograms (Figure 1a), there is an absence (or neglectable amounts) of secondary phases in pristine FeS_2 and FeS_2 with Co and Se-(Co,Se)-FeS_2. There is a small amount of NiS_2 in pyrite with Ni and Se - (Ni,Se)-FeS_2. Most of the peaks in CoSbS XRD diffractograms (Figure 1b) are indexed to the phase paracostibite, although there is also Sb_2S_3 (stibnite) and β-CoS. The synthesis of these sulfides resulted in highly porous pellets, easily desegregated. Since the measurement of electrical transport properties requires highly compact materials, further densification was carried by hot-pressing.

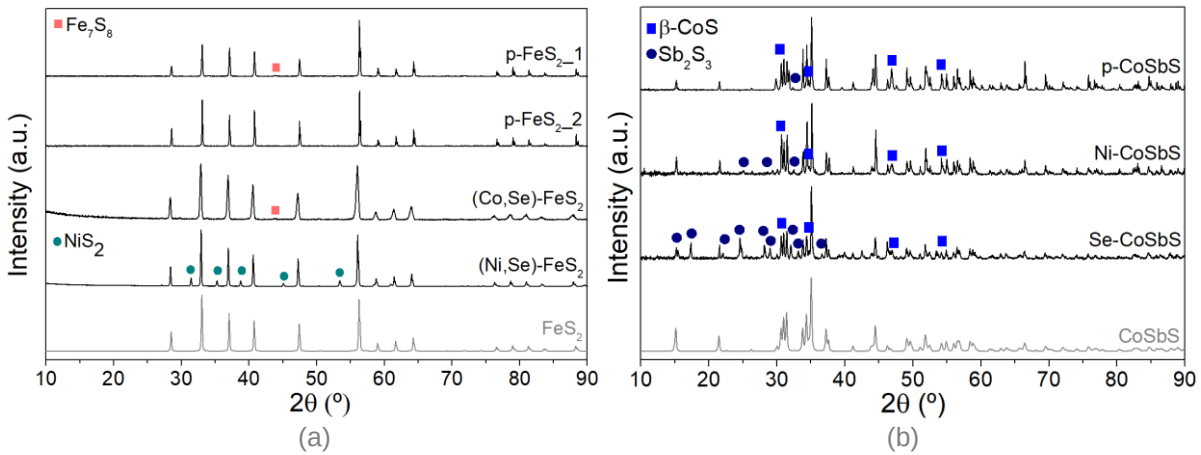

(a) (b)

Figure 1 – XRD diffractograms of pyrite compositions (a) and paracostibite compositions (b).

3.2. Densification by hot-pressing

The consolidation of the sulfides to be studied required an initial parameter optimization. After several attempted conditions (see Table 1), it was concluded that the parameters that promote a higher densification of pristine FeS_2 are 710ºC and 60MPa for 1,5h (relative density of ~95% and 14±3% of porosity). The modification of pyrite initial composition promoted the densification at lower pressures. For (Co,Se)-FeS_2 and (Ni,Se)-FeS_2, it was obtained a density of ~93% and ~95% (3.6±0.3% and 1.9±0.6% of porosity), respectively, at 710ºC and 49MPa for 1,5h. The denser pellet of NiS_2 was obtained at 750ºC and 56MPa for 1,5h, achieving a relative density of ~97% and 4±1% of porosity. Paracostibite was better densified at 725ºC, 49MPa for 1,25h (~96% of relative density and 1.1±0.8% porosity). The first two consolidation conditions resulted in single phase pellets, except for pyrite with substitutions. (Co,Se)-FeS_2 and (Ni,Se)-FeS_2 presented Fe_7S_8 and NiS_2, respectively. In paracostibite, it was required a heat-treatment at 720ºC for 7 days to homogenize the chemical composition. The heat-treated samples still had a significant amount of β-CoS, but in lower amount (8, 12 and 30vol%, respectively, for p-CoSbS, Ni-CoSbS and Se-CoSbS). In p-CoSbS, the heat-treatment had an undesired effect of increasing the porosity (percentage of pores increased to 10.2±0.6% and relative density decreased to ~83%). SEM images of hot-pressed samples are shown in Figure 2. The lattice constants of pristine FeS_2 and NiS_2, for all consolidation conditions, are in good agreement with the literature values for powdered FeS_2 (a = 5.416-5.418 Å) and NiS_2 (a= 5.687-5.688) [17]. The substitution of Se and Co or Ni in pyrite structure increased the lattice constant, from 5.418 Å to ~5.431-5.433 Å.

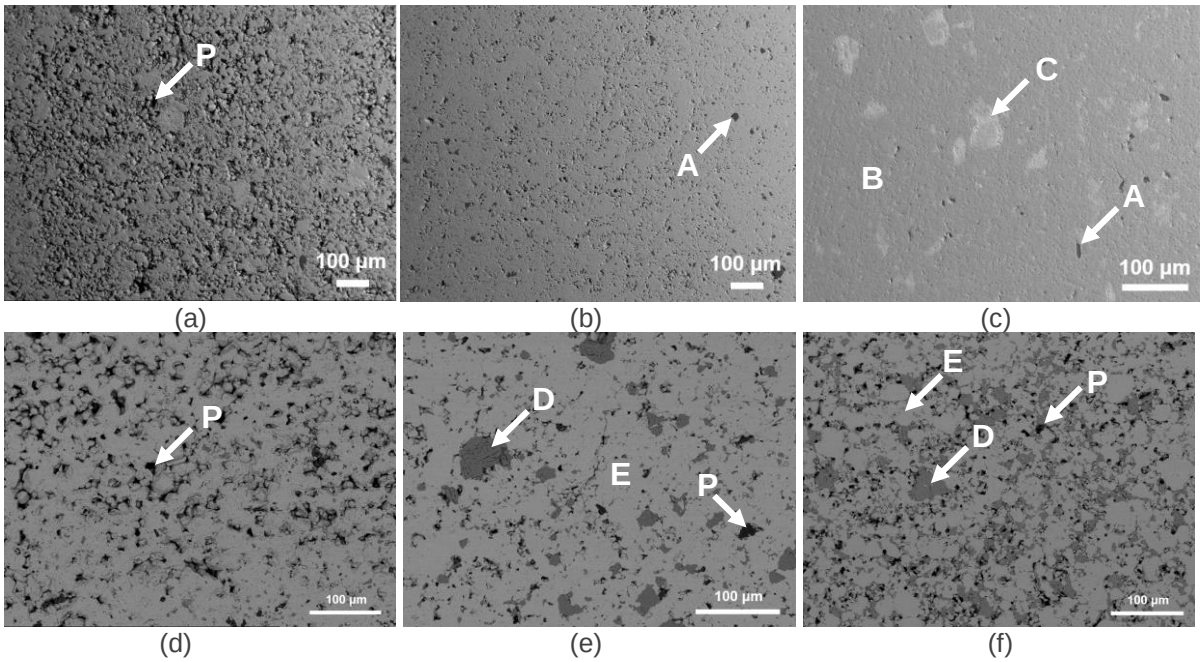

Figure 2 – SEM images after consolidation of: (a) FeS2, (b) NiS2, (c) (Ni,Se)-FeS2, (d) CoSbS, (e) Ni-CoSbS and (f) Se-CoSbS. P – Pores, A – SiO2, B – FeS2-xSex , C – NiS2-xSex with Fe, D – β-CoS, E - CoSbS.

The cell parameters of the phase paracostibite, both after consolidation and heat-treatment, fall within the range of values reported in the literature [17]. After heat-treatment, an increase of the lattice parameters occurred with the substitutions of either Ni or Se on Co and S sites, respectively, when compared with pristine CoSbS.

The EDS results revealed a metallic cation:sulfur ratio of, approximately, 1:1.9, 1:2 and 1:1:1, for pristine FeS_2, NiS_2 and CoSbS, respectively, which is close from the intended. In (Co,Se)-FeS_2, the substitution of 10at% Co in pyrite was successful. On the other hand, only ~10at% of Se was substituted on S sites, instead of the 12.5at% intended, result of the difficulty in controlling the extension of chalcogenides evaporation during hot-pressing. In (Ni,Se)-FeS_2, two different phases are present: pyrite with Se on S sites ($FeS_{1.98\pm0.02}Se_{0.09\pm0.04}$), and vaesite with Fe and Se. In vaesite hot-pressed at 700ºC and 750ºC, there is also a sulfur-deficient secondary phase (NiS), only detected by SEM/EDS (<1vol%). In paracostibite samples, the secondary phase (region C) has a stoichiometry close from 1:1, corresponding to β-CoS. In Ni-CoSbS, EDS did not detect Ni in the paracostibite phase, meaning that either there was no substitution of Ni on Co sites or a scarce incorporation of Ni occurred (below the limit of detection of the equipment). However, it was detected Ni in β-CoS, with a partial substitution of Ni on ~7at% of Co sites. EDS results revealed the presence of Se in both phases of Se-CoSbS. A substitution of ~9at%Se and 5at%Se occurred in paracostibite and β-CoS, respectively. The presence β-CoS in all these samples evidence that CoSbS is decomposing into β-CoS and a liquid phase at temperatures lower than reported by Allazov et al. [19].

In the Raman spectra of pristine FeS_2 (Figure 3a), hot-pressed at 710ºC and 49MPa, , it is visible four out of five pyrite vibrational modes [20, 21]: E_g at 335 cm^{-1}, $T_g(1)$ at 339 cm^{-1}, A_g at 368 cm^{-1}, and $T_g(3)$ at 420 cm^{-1}. In pyrite hot-pressed at 710ºC and 60MPa (Figure 3b) there is a subtle deviation of the peaks to the right, suggesting that a higher hot-pressing pressure shortens the S-S bonds. Raman spectra of (Co,Se)-FeS_2 (Figure 3c) shows broader peaks, shifted to the left. This result proves that the substitution of larger and heavier atoms (Se and Co) on S and Fe sites, respectively, increased the disorder in the crystal lattice and induced tensile stresses.

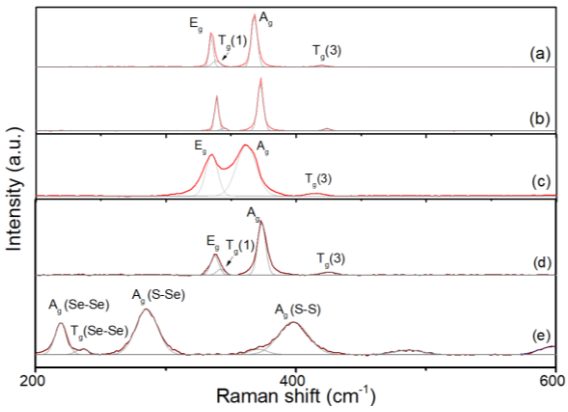

Figure 3 – Raman spectra of hot-pressed (a) FeS2_49_710; (b) FeS2_60_710; (c) (Co,Se)-FeS2; (d) (Ni,Se)-FeS2, region B; (e) (Ni,Se) FeS2 , reg. C.

Raman spectra of (Ni,Se)-FeS_2 corroborates the previous results in the sense that this sample has an inhomogeneous microstructure with two phases: one with S-S vibrational modes characteristic of pyrite (Figure 3d), and another corresponding to $NiS_{2-x}Se_x$ (Figure 3e).

The Raman spectra of hot-pressed NiS_2, for different consolidation conditions, have only four peaks, instead of the expected five [21, 22]: two smaller peaks at 268 and 278 cm^{-1}, which correspond to the pair librations ($T_g(1)$ and E_g); a more intense peak at 474 cm^{-1}, which corresponds to the in-phase stretching of S-S

bonds (A_g); and a shoulder at 485 cm^{-1}, corresponding to $T_g(2)$ mode. The fifth Raman active mode, $T_g(3)$, not visible in the spectra, has never been reported in previous Raman data literature. The similarity of the Raman spectra for different samples, in terms of peak positions and width, suggests that the different consolidation conditions or the presence of NiS did not cause any apparent distortion or strain in their lattice.

Raman spectroscopy of CoSbS samples was inconclusive. One can at least conclude that most of the peaks are correlated with Sb-Sb, Sb-S and S-S vibrational modes, since they fit within the range 100-350cm^{-1} where these peaks are found in other antimony-sulfur compounds with similar crystal structure.

3.3. Thermal stability

Thermal stability, under inert atmosphere, of the sulfides of interest was ascertained from room temperature to 900ºC. TGA curve of pyrite (Figure 4) shows signs of oxidation in the as-synthesized FeS_2. Pristine FeS2 and pyrite with Ni and Se start losing their mass at ~360ºC, whereas pyrite with Co and Se only starts to

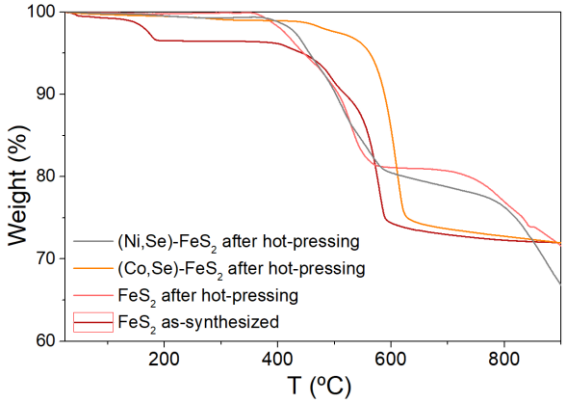

Figure 4 – TGA curve of FeS2, before and after hot-pressing, under inert atmosphere.

desulfurize at 430ºC, meaning that this composition modification could be beneficial to retain sulfur in pyrite structure. At 900ºC, the percentage of lost mass due to sulfur evaporation is ~24% for as-synthesized FeS_2, ~27% for hot-pressed pristine FeS_2 and FeS_2 with Co and Se, and 33% for FeS_2 with Ni and Se. The mechanisms of pyrite decomposition have been previously studied by Lambert et al. (release of sulfur from pyrite lattice, decomposition of FeS_2 into $Fe_{1-x}S$ and decomposition of $Fe_{1-x}S$ into FeS) [23].

TG analysis of NiS_2 (Figure 5) reveals a loss of 35% of the mass due to desulfurization, which starts to occur at 340ºC in hot-pressed NiS_2 and 440ºC in as-synthesized powders.

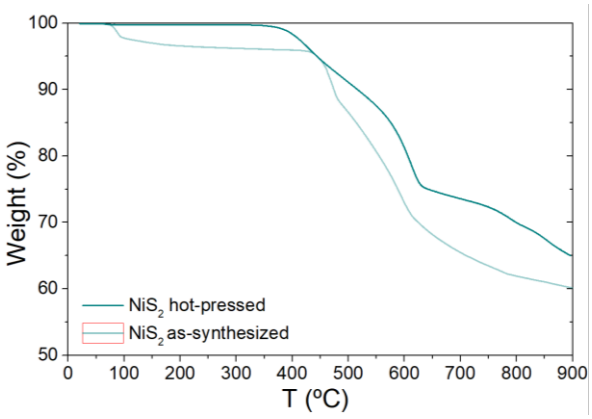

Figure 5 – TGA curve of NiS2, before and after hot-pressing, under inert atmosphere.

The early loss of sulfur in hot-pressed NiS_2 is most likely related with the excess of sulfur added prior the hot-pressing. If not all the sulfur in excess has been evaporated during hot-pressing, it will be more readily released from vaesite lattice throughout the TG heating cycle. There are no previous studies on the mechanisms of decomposition of vaesite but the similarity of with pyrite TGA results suggests that NiS2 might decompose by similar mechanisms.

The TGA curves of paracostibite (Figure 6), with and without substitutions, exhibit a good thermal stability until 800ºC. Above 800ºC, all samples

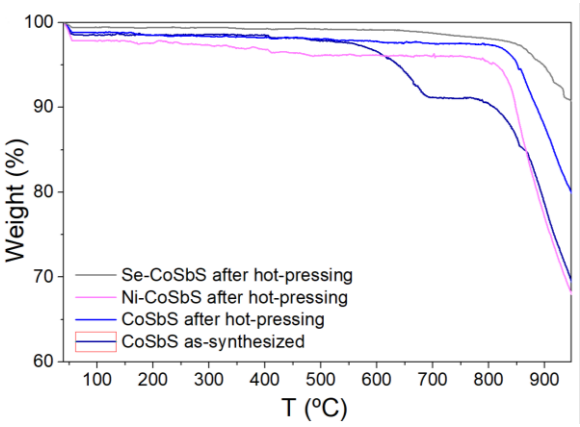

Figure 6 – TGA curve of CoSbS-based samples, under inert atmosphere.

suffer a steep mass loss, more accentuated in Ni-CoSbS (~ 29% of its weight is lost), and less felt in Se-CoSbS (~ 9% of mass lost). This mass drop is associated with the occurrence of a peritectic reaction, which starts at 700-795ºC. The decomposition of CoSbS into β-CoS and liquid is most likely accompanied with the evaporation of sulfur and sulfur-antimony compounds. The as-synthesized CoSbS powder has a weight drop around 550-680ºC, corresponding to the evaporation of Sb_2S_3, reported to occur from 545ºC to 768ºC [24]. Paracostibite is less prone to desulfurization than pyrite and vaesite.

3.4. Electronic transport properties

The calculated band structure and density of states are shown in Figure 7. DFT calculations indicate that pyrite and paracostibite are indirect band gap p-type semiconductors. The calculated band gap energies (1.14eV for FeS_2, 0.76eV for CoSbS) are slightly overestimated when compared with experimental E_g values (0.9-0.95 eV for FeS_2, 0.5-0.75eV for CoSbS) [6, 12]. The presence of multiple peaks in the valence band, added to the low dispersion of the bands near the Fermi level, that results in a steep increase of DOS in that region, suggest that FeS_2 and CoSbS might have a high power factor (α^2/ρ). Substitution of Co and Ni on Fe sites increases the concentration and mobility of the charge carriers. Substitution of Se on S sites increases the degeneracy of the valence band, enhancing the power factor [13, 25].

From the DFT calculations, one could expect NiS_2 to be metallic due to the partly filled e_g band. However, experimental data points to a semiconductor behavior, due to its Mott insulator behavior, that induces strong correlation effects that are not predicted by conventional band theories. The bandgap of vaesite has been reported to be 0.27eV [26].

The Seebeck coefficient of bulk pyrite and paracostibite is negative (n-type semiconductivity). These results contradict the DFT calculations that pointed to p-type conductivity. A maximum power factor at room temperature, of 105.5 $\mu WK^{-2}m^{-1}$ was achieved for pyrite with Co and Se. However, its semi-metallic behavior suggests that this high power factor might be accompanied by an high thermal conductivity, leading to a substantial decrease of zT. The maximum power factor measured in pristine FeS_2 was 0.2 $\mu WK^{-2}m^{-1}$. Paracostibite power factor at room temperature was 34 $\mu WK^{-2}m^{-1}$, achieving a maximum of 72 $\mu WK^{-2}m^{-1}$, in paracostibite with Ni. In vaesite, it was achieved a maximum power factor of 14.1 $\mu WK^{-2}m^{-1}$. The consolidation conditions had a notable influence on the resistivity, with denser pellets showing a higher electrical conduction. The electronic transport properties seem to be related with defects (stoichiometric deviations, grain boundaries) and changes in the chemical composition.

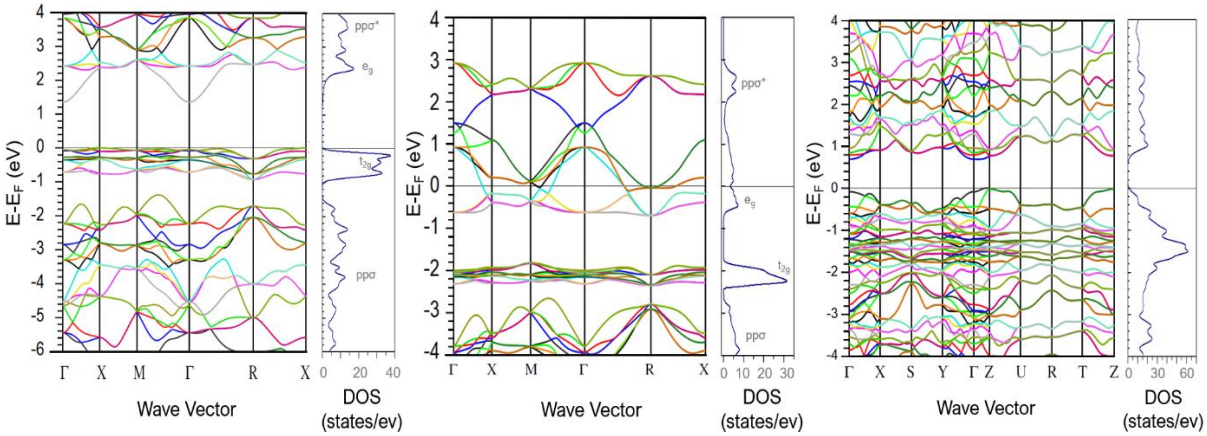

(a) (b) (c)

Figure 7 - Electronic band structure and density of states of (a) FeS2, (b) NiS2 and (c) CoSbS, calculated by WIEN2k.

Table 2 – Seebeck coefficient (α), electrical resistivity (ρ) and power factor (PF) at 300K.

Sample	Processing conditions	α (μV/K)	ρ (μΩm)	PF (μWK^{-2}m^{-1})
p-FeS_2	HP 710ºC, 1.5h, 49MPa	-40	7018	0.2
(Co,Se)-FeS_2	HP 710ºC, 1.5h, 49MPa	-59	33	105.5
(Ni,Se)-FeS_2	HP 710ºC, 1.5h, 49MPa	-21	1020	0.4
NiS_2_56_700	HP 700ºC, 1.5h, 56MPa	128	3230	5.1
NiS_2_56_720	HP 720ºC, 1.5h, 56MPa	182	2350	14.1
NiS_2_56_750	HP 750ºC, 1.5h, 56MPa	119	2257	6.3
p-CoSbS	HP 725ºC, 1.25h, 49MPa + HT 720ºC, 7 days	-176	911	34
Ni-CoSbS	HP 725ºC, 1.25h, 49MPa + HT 720ºC, 7 days	-69	66	72
Se-CoSbS	HP 725ºC, 1.25h, 49MPa + HT 720ºC, 7 days	-79	433	14

4. Conclusions and future work

The preparation by solid-state route, followed by hot-pressing resulted in FeS_2 and NiS_2 single phase pellets. In paracostibite, it was required a heat-treatment at 720ºC for 7 days to homogenize the chemical composition. The modification of the initial composition of these compounds has a substantial influence on the densification process. In general, relative densities superior to 90% were achieved, except for pristine CoSbS (82%). Even heat-treated, paracostibite still had regions of β-CoS (8%vol for pristine CoSbS, 12%vol for CoSbS with Ni, and 30%vol for CoSbS with Se). Unlike Se, Ni was not successfully incorporated in CoSbS structure. The presence of β-CoS indicates that, under non-equilibrium conditions, the peritectic reaction starts to occur at lower temperatures than previously reported in the literature. No significant changes in chemical bonds and lattice distortions were verified for different hot-pressing conditions. However, the substitution for heavier atoms lead to a considerable disorder of the lattice. Thermogravimetric analysis of these compounds indicates a strong desulfurization in all sulfides, which limits their service temperature to 360ºC (FeS_2, NiS_2), 430ºC (FeS_2 with Co) and 750-800ºC (CoSbS). The preparation of pyrite by solid-state reaction followed by hot-pressing resulted in a low power factor. The successful incorporation of Co and

Se in pyrite structure proved to be an interesting strategy to improve the power factor, even though the quantities of each element need further tuning in order to keep the semiconducting behavior. The modest power factors of vaesite and paracostibite are a good starting point for further improvement. With a proper optimization of the chemical composition and microstructure, these sulfides could turn into viable thermoelectric materials. Several aspects were left unexplored in this work. Since the potential of a material for thermoelectricity is also related with its thermal transport properties, a further study of the thermal conductivity is required. The selection of the optimal chemical composition of vaesite and paracostibite is also necessary. The coupling of these materials in a thermoelectric module also demands good mechanical properties, which so far were never studied. In this project, the thermal stability under inert atmosphere was studied but it would be interesting to evaluate the stability in air (oxidation testing).

References

[1] World Energy Council, *Energy Efficiency Indicators* (2016), https://wec-indicators.enerdata.net/ratio-final-primary-intensity.html, acessed on 01-06-2019.

[2] A. P. Gonçalves and C. Godart. *European Physical Journal B,* 87 (42), 2014.

[3] Z. H. Ge, L. Zhao, D. Wu, X. Liu, B. Zhang, J. Li and J. He. *Materials Today,* 19(4): 227-239, 2016.

[4] R. Sun, M. Chan and G. Ceder. *Physical Review B,* 83: 235311, 2011.

[5] G. Krill, M. F. Lapierre, F. Gautier, C. Robert, G. Czjzek, J. Fink and H. Schmidt. *Journal of Physics C: Solid State Physics,* 9: 761-782, 1976.

[6] C. Uhlig, E. Guenes, A. S. Schulze, M. T. Elm, P. J. Klar and S. Schlecht. *Journal of Electronic Materials,* 19 (4): 2362-2370, 2014.

[7] J. M. Clamagirand, J. R. Ares, I. J. Ferrer and C. Sánchez. *AIP Conference Proceedings 1449,* 183, 2012.

[8] B. T. Bither, R. J. Bouchard, W. H. Cloud, P. C. Donohue and W. J. Siemons. *Inorganic Chemistry,* 7(11): 2208-2220, 1968.

[9] L. J. Cabri, D. C. Harris and J. M. Stewart. *The Canadian Mineralogist,* 10(2): 232-246, 1970.

[10] Z. Liu, H. Geng, J. Shuai, Z. Wang, J. Mao, D. Wang, Q. Jie, W. Cai, J. Sui and Z. Ren. *Journal of Materials Chemistry C,* 3: 10442-10450, 2015.

[11] R. Chimieloski, S. Battacharyab, W. Xiec, D. Péréa, S. Jacoba, R. Sternb, K. Moriyaa, A. Weidenkaffc, G. K. H. Madsenb and G. Dennlera. *Journal of Materials Chemistry C,* 4: 3094-3100, 2016.

[12] D. Parker, A. F. May, H. Wang, M. A. McGuire, B. C. Sales and D. J. Singh. *Physical Review B,* 87: 045205, 2013.

[13] W. Yao, D. Yang, Y. Yan, K. Peng, H. Zhan, A. Liu, X. Lu, G. Wang and X. Zhou. *ACS Applied Materials and Interfaces,* 9(12): 10595-10601, 2017.

[14] T. J. B. Holland and S. A. T. Redfern. *Mineralogical Magazine,* 61: 65-77, 1996.

[15] P. M. Chaikin and J. F. Kwak. *Review of Scientific Instruments,* 46(218), 1975.

[16] P. Blaha, K. Schwarz, G. K. H. Madsen, D. Kvasnicka, J. Luitz, R. Laskowski, F. Tran and D. Marks. *WIEN2k - An AUgmented Plane Wave + Local Orbitals Program for Calculating Crystal Properties*, 2018.

[17] P. Villars and L. D. Calvert, *Pearson's Handbook of Crystallographic Data for Intermetallic Phases*, American Society for Metals, 1986.

[18] J. P. Perdew, K. Burke and M. Ernzerhof. *Physical Review Letter,* 77: 3865, 1996.

[19] M. R. Allazov and Z. T. Gulieva. *Zhurnal Neorganicheskoi Khimii,* 33(7): 1887-1891, 1988.

[20] A. N. Utyuzh. *Physics of the Solid State,* 56(10): 2050-2055, 2014.

[21] C. Heras and F. Agulló-Rueda. *Journal of Physics: Condensed Matter,* 12: 5317-5324, 2000.

[22] C. Marini, A. Perucchi, D. Chermisi, P.Dore, M. Valentini, D. Topwal, D. D. Sarma e S. Lupi. *Physical Review B,* 84: 235134, 2011.

[23] J. M. Lambert, G. Simkovich e J. P. L. Walker. *Metallurgical and Materials Transactions B,* 29B(2): 385-396, 1998.

[24] R. Padilla, G. Ramirez e M. C. Ruiz. *Metallurgical and Materials Transactions B,* 41B: 1284-1292, 2010.

[25] Y. You, X. Su, S. Hao, W. Lu, Y. Yan, T. Zhang, M. Zhang, C. Wolverton, M. G. Kanatzidis e X. Tang. *Journal of Materials Chemistry A,* 6: 15123-15131, 2018.

[26] R. L. Kautz, M. S. Dresselhaus, D. Adler e A. Linz. *Physical Review B,* 6(6): 2078-2082, 1972.

[27] F. Gautier, G. Krill, M. F. Lapierre and C. Robert. *Solid State Communications,* 11: 1201-1203, 1972.